bioRxiv preprint doi: https://doi.org/10.1101/2020.10.16.342378; this version posted October 16, 2020. The copyright holder for this preprint (which was not certified by peer review) is the author/funder, who has granted bioRxiv a license to display the preprint in perpetuity. It is made available under aCC-BY 4.0 International license.

Beyond broadband: towards a spectral decomposition of EEG microstates

Victor Férat [1], Martin Seeber [1], Christoph M. Michel [1,2], Tomas Ros [1,2]

1 Functional Brain Mapping Laboratory, Department of Basic Neurosciences, Campus Biotech, University of Geneva, Geneva, Switzerland

2 Centre for Biomedical Imaging (CIBM) Lausanne-Geneva, Geneva, Switzerland

Keywords: EEG ; microstates; topography; Resting state ; eyes closed ; eyes open ; alpha; mutual information

Highlights:

- Microstate topographies are similar across standard EEG bands.
- The temporal dynamics of microstate topographies are independent across standard EEG bands
- Band-specific microstate analysis may reveal more specific and/or novel effects compared to broadband microstate analysis

Abstract

Microstate (MS) analysis takes advantage of the electroencephalogram's (EEG) high temporal resolution to segment the brain's electrical potentials into a temporal sequence of scalp topographies. Originally applied to alpha oscillations in the 1970s, MS analysis has since been used to decompose mainly broadband EEG signals (e.g. 1-40 Hz). We

bioRxiv preprint doi: https://doi.org/10.1101/2020.10.16.342378; this version posted October 16, 2020. The copyright holder for this preprint (which was not certified by peer review) is the author/funder, who has granted bioRxiv a license to display the preprint in perpetuity. It is made available under aCC-BY 4.0 International license.

hypothesized that MS decomposition within separate, narrow frequency bands could provide more fine-grained information for capturing the spatio-temporal complexity of multichannel EEG. In this study using a large open-access dataset (n=203), we pre-filtered EEG recordings into 4 classical frequency bands (delta, theta, alpha, beta) in order to compare their individual MS segmentations using mutual information as well as traditional MS measures. Firstly, we confirmed that MS topographies were spatially equivalent across all frequencies, matching the canonical broadband maps (A, B, C, and D). Interestingly however, we observed strong informational independence of MS temporal sequences between spectral bands, together with significant divergence in traditional MS measures (e.g. mean duration, time coverage). For instance, MS sequences in the alpha-band exhibited temporal independence from sequences in all other frequencies, whilst also being longer on average (>100 ms). Based on a frequency vs. map taxonomy (e.g. ΘA, αC, βB), narrow-band MS analyses revealed novel relationships that were not evident from the coarse-grained broadband analysis. Overall, our findings demonstrate the value and validity of spectral MS analysis for decomposing the full-band EEG into a richer palette of frequency-specific microstates. This could prove useful for identifying new neural mechanisms in fundamental research and/or for biomarker discovery in clinical populations.

bioRxiv preprint doi: https://doi.org/10.1101/2020.10.16.342378; this version posted October 16, 2020. The copyright holder for this preprint (which was not certified by peer review) is the author/funder, who has granted bioRxiv a license to display the preprint in perpetuity. It is made available under aCC-BY 4.0 International license.

1 Introduction

Multi-channel Electroencephalography (EEG) is a long-established tool for exploring the human brain's spatio-temporal activities. Microstate (MS) analysis [1] , first introduced by Lehmann [2] in 1971, takes advantage of EEG's high temporal resolution to segment EEG signals into short successive periods of time characterized by metastable scalp topographies. Initially applied to narrow-band alpha oscillations (8 -12 Hz)[2], microstate analysis is nowadays usually performed on broadband EEG signals (1 – 40Hz) [1], [3]. Historically, only a limited number of studies [4]–[6] have focused on applying MS analysis to the traditional frequencies associated with cortical oscillations (e.g. delta, theta, alpha, beta etc.). For example, in the 1990's, Merrin et al [4] were the first to report on a significant difference in MS segments between schizophrenic patients and controls specifically in the theta EEG band. On the other hand, more recent work in healthy subjects found that MS dynamics were independent of EEG power fluctuations across the frequency spectrum [7], which technically supported the rationale for performing broadband MS analysis. Neuroimaging studies have nevertheless emerged showing that anatomically-distinct cortical regions display different dominant EEG frequencies, with occipito-parietal regions more active in the alpha band, and prefrontal regions being biased more toward delta or theta power [8]–[10]. Moreover, ongoing cortical dynamics have been reported to fluctuate from a local resting/idling alpha oscillatory state to task-specific active mode(s) dominated by other rhythms (e.g. theta [11], gamma [12]). As a consequence, cortical regions could combine different frequencies for integrating/segregating information across large-scale networks, a phenomenon termed "oscillatory multiplexing" [13]. Finally, of more clinical significance, a growing body of work has indicated abnormal EEG

bioRxiv preprint doi: https://doi.org/10.1101/2020.10.16.342378; this version posted October 16, 2020. The copyright holder for this preprint (which was not certified by peer review) is the author/funder, who has granted bioRxiv a license to display the preprint in perpetuity. It is made available under aCC-BY 4.0 International license.

spectral power in distinct frequencies across cortical regions in a variety of brain disorders [14], [15]. Therefore, given that different spatial topographies uncovered by MS analysis imply anatomically-distinct cortical generators (according to the forward-model of EEG generation [1]), it is reasonable to hypothesize that distinct MS topographies may display different spatial and/or temporal profiles across the frequency spectrum.

To investigate this question as well as gain a deeper understanding of frequency-specific MS signature(s), we sought to explicitly decompose MS spatio-temporal dynamics within *discrete, narrow-band frequency bands* (i.e. delta, theta, alpha, and beta), with the aim of comparing them to the classical analysis of the broadband signal.

Here, we employed a validated, open-source dataset [16] of resting-state EEG recordings from 203 healthy subjects during both eyes opened and eyes closed conditions. These were then filtered in the classical EEG bands (delta: 0-4 Hz, theta: 4-8 Hz, alpha: 8-12 Hz, beta: 15-30 Hz) to obtain band specific signals. These narrow-band signals, in addition to the broadband (1-30 Hz) signal, were then independently subjected to standard microstate analysis [17]. Map topography, mean duration, occurrence, time coverage, and global explained variance (GEV) were used as quantitative measures of spatiotemporal microstate dynamics. In summary, and using spatial correlation analysis, we firstly demonstrate remarkably similar microstate topographies across frequencies, closely matching the classical broadband maps. Interestingly, however, we observed strong informational independence of microstate sequences between frequencies, in addition to significant differences in established measures of temporal dynamics (mean duration, occurrence, and time coverage).

bioRxiv preprint doi: https://doi.org/10.1101/2020.10.16.342378; this version posted October 16, 2020. The copyright holder for this preprint (which was not certified by peer review) is the author/funder, who has granted bioRxiv a license to display the preprint in perpetuity. It is made available under aCC-BY 4.0 International license.

In conclusion, our results support a more diverse, frequency-specific application of microstate analysis compatible with the narrow-band MS analyses of early pioneers [2], [4]. We anticipate this approach to provide a more fine-grained spectral information not visible to the standard broadband analysis, for example in the identification of biomarkers in clinical populations or for understanding the mechanisms underlying EEG microstates.

2 Methods

2.1 Dataset

EEG recordings were obtained from 203 anonymized participants enrolled in the Mind-Brain-Body study [16]. Detailed protocol and inclusion criteria are reported in [16]. The overall sample consisted of 227 participants divided into 2 groups: the younger adults group with participant age ranging between 20 and 35 years (N = 153, 45 females, mean age = 25.1 years, SD = 3.1) and an older adults group with age ranging between 59 and 77 years (N = 74, 37 females, mean age = 67.6 years, SD = 4.7). Medical and psychological screening was conducted on all participants at the Day Clinic for Cognitive Neurology of the University Clinic Leipzig and the Max Planck Institute for Human and Cognitive and Brain Sciences in order to include only healthy patients. The study protocol was approved by the ethics committee of the University of Leipzig (reference

154/13-ff). Data were obtained in accordance with the Declaration of Helsinki.

bioRxiv preprint doi: https://doi.org/10.1101/2020.10.16.342378; this version posted October 16, 2020. The copyright holder for this preprint (which was not certified by peer review) is the author/funder, who has granted bioRxiv a license to display the preprint in perpetuity. It is made available under aCC-BY 4.0 International license.

2.2 Recordings

Resting state EEGs were recorded using 61 scalp electrodes (ActiCAP, Brain Products GmbH, Gilching, Germany), and one additional VEOG electrode for recording right eye activity. All electrodes were placed according to the international standard 10–20 extended localization system with FCz reference, digitized with a sampling frequency of fs=2500 Hz,an amplitude resolution of 0.1 microV ,and bandpass filtered between 0.015Hz and 1 kHz. The ground was located at the sternum and scalp electrode impedance was kept below 5 KΩ. Recordings took place in an electrically shielded and sound-attenuated EEG booth. Here, 60s blocks alternated between eyes open (EO) and eyes closed (EC) conditions for a total recording of 16 min (8 blocks EC, 8 blocks EO, starting with EC). During the EO condition, participants were asked to stay awake while fixating their eyes on a black cross presented on a white background.

2.3 Prepocessing

The prepossessing steps are extensively described in [16], which we summarize below. All EEG recordings were down-sampled from 2500 to 250 Hz and filtered between 1 and 45Hz (8th order, Butterworth filter). Blocks sharing the same condition were concatenated leading to the creation of 2 datasets per subject. After visual inspection, outlying channels were rejected and EEG segments presenting noise and/or artefacts were removed (except eye movements and eye blinks that were kept for further prepossessing). PCA was used to reduce data dimensionality, by keeping PCs (N≥30) that explain 95% of the total data variance. Then, independent component analysis (ICA) was performed

bioRxiv preprint doi: https://doi.org/10.1101/2020.10.16.342378; this version posted October 16, 2020. The copyright holder for this preprint (which was not certified by peer review) is the author/funder, who has granted bioRxiv a license to display the preprint in perpetuity. It is made available under aCC-BY 4.0 International license.

using the Infomax (runica) algorithm. Components reflecting eye movement, eye blink or heartbeat related artefacts were removed.

Before performing microstate analysis, the following additional prepossessing steps were conducted using MNE-python [18]: missing/bad channels were interpolated using spherical spline interpolation, the reference was re-projected to average and recordings were down-sampled to 100Hz. Finally, each recording was filtered into broadband plus the 5 traditional EEG frequency bands: broadband (1-30 Hz), delta (1-4 Hz), theta (4-8 Hz), alpha (8-12 Hz), beta (15-30 Hz). Filter design consisted of a two-pass forward and reverse, zero-phase, non-causal band-pass FIR filter with the following parameters.

Broadband: - Lower passband edge: 1.00 - Lower transition bandwidth: 1.00 Hz (-12 dB cutoff frequency: 0.50 Hz) - Upper passband edge: 30.00 Hz

- Upper transition bandwidth: 7.50 Hz (-12 dB cutoff frequency: 33.75 Hz) Filter length: 331 samples (3.310 sec)

Delta: - Lower passband edge: 1.00 - Lower transition bandwidth: 1.00 Hz (-12 dB cutoff frequency: 0.50 Hz) - Upper passband edge: 4.00 Hz - Upper transition bandwidth: 2.00 Hz (-12 dB cutoff frequency: 5.00 Hz) - Filter length: 331 samples (3.310 sec)

Theta: - Lower passband edge: 4.00 - Lower transition bandwidth: 2.00 Hz (-12 dB cutoff frequency: 3.00 Hz) - Upper passband edge: 8.00 Hz - Upper transition bandwidth: 2.00 Hz (-12 dB cutoff frequency: 9.00 Hz) - Filter length: 165 samples (1.650 sec)

Alpha: - Lower passband edge: 8.00 - Lower transition bandwidth: 2.00 Hz (-12 dB cutoff frequency: 7.00 Hz) - Upper passband edge: 12.00 Hz - Upper transition bandwidth: 3.00 Hz (-12 dB cutoff frequency: 13.50 Hz) - Filter length: 165 samples (1.650 sec)

bioRxiv preprint doi: https://doi.org/10.1101/2020.10.16.342378; this version posted October 16, 2020. The copyright holder for this preprint (which was not certified by peer review) is the author/funder, who has granted bioRxiv a license to display the preprint in perpetuity. It is made available under aCC-BY 4.0 International license.

Beta: - Lower passband edge: 15.00 - Lower transition bandwidth: 3.75 Hz (-12 dB cutoff frequency: 13.12 Hz) - Upper passband edge: 30.00 Hz - Upper transition bandwidth: 7.50 Hz (-12 dB cutoff frequency: 33.75 Hz) - Filter length: 89 samples (0.890 sec)

For all filters, a Hamming window with 0.0194 passband ripple and 53 dB stopband attenuation was used to reduce border effects.

2.4 MS segmentation

2.4.1 Segmentation

Microstate segmentation was applied to each combination of frequency band (broadband, delta, theta, alpha, beta) x behavioural condition (EO, EC) leading to the computation of 10 optimal clusters using the methodology described below. First, local maxima of the Global Field Power (GFP) known to represent portions of EEG data with highest signal to noise ratio [19], were extracted from each individual recording. Then, 20 epochs of 500 time points randomly drawn from the previous extraction were submitted to a modified k-means cluster analysis using the free academic software Cartool [20]. For each number of cluster centers K ranging from 1 to 12, 50 k-means initialisations were applied to each epoch. The initialisation with highest global explained variance (GEV) was selected and kept for further processing. A meta-criterion [21] was used to choose the optimal number of cluster centers k for each epoch. Individual optimal clusters were then merged within conditions and within frequencies to form 10 groups of 4060 clusters. Each group was then randomly re-sampled into 100 epochs of 5000 time points, and submitted to the same clustering algorithm (50 initialisations, with meta criterion selection), leading to the extraction of 100 optimal clusters per group. Finally, these 100 clusters were submitted to the modified K means

bioRxiv preprint doi: https://doi.org/10.1101/2020.10.16.342378; this version posted October 16, 2020. The copyright holder for this preprint (which was not certified by peer review) is the author/funder, who has granted bioRxiv a license to display the preprint in perpetuity. It is made available under aCC-BY 4.0 International license.

clustering algorithm to extract, for each number of cluster centroids k, a set of maps which best represent the spatiotemporal variance of frequency specific EEG data within each condition.

Selection of "common" MS maps

Given that we found high spatial correlations between MS maps across all frequencies and EO/EC conditions, we fitted the broadband maps directly to all the frequency bands in order to have a common reference. This may be considered a heuristic approach for the sake of simplicity. An alternative approach we explored was to perform subject-level (i.e. 1st level) clustering on all data concatenated *within-subject* (across frequencies, and/or conditions), followed by group-level (i.e. 2nd-level) clustering. We found this to once again produce identical maps to the broadband decomposition. This method could theoretically be used to find the most "common" clusters across different datasets, in case of variable k-means outputs (e.g. visually similar MS maps at different k-values). Since it is beyond the scope of this paper, we leave it to future studies to validate this method more rigorously.

2.4.2 Fitting

The common topographic maps selected above were then assigned to every time point from all individual recordings using the traditional MS back-fitting method [22]. First, the spatial correlation was computed between every timepoint and map. Using the so called 'winner takes all' algorithm, each timepoint was labelled according to the map with which it shared the highest absolute spatial correlation. Timepoints were labelled as "non-assigned" when the absolute spatial correlation was below $r < 0.5$ threshold. To ensure temporal continuity of MS segmentation, a

bioRxiv preprint doi: https://doi.org/10.1101/2020.10.16.342378; this version posted October 16, 2020. The copyright holder for this preprint (which was not certified by peer review) is the author/funder, who has granted bioRxiv a license to display the preprint in perpetuity. It is made available under aCC-BY 4.0 International license.

smoothing step [17], [20] was applied. Finally, segments with duration shorter than 3 samples (30ms) were assigned to neighbouring segments using the following rule: the segment was split into two parts, where each part was assigned to the neighbouring segment with the higher spatial correlation. With backfitting completed, we extracted 4 spatiotemporal parameters for each microstate map, namely:

Global explained variance (Gev) described as the sum of variances of the original recording explained by the considered microstate map weighted by the Global Field Power at each moment in time. Units are percentages (%) between 0 and 1.

Mean spatial correlation (MeanSpatCorr) defined as the mean spatial correlation value between the assigned MS map and actual scalp topography at each timepoint. This results in a correlation coefficient $0 \leq r \leq 1$.

Mean duration (MeanDurs), defined as the mean temporal duration of segments assigned to each MS map. Units are in seconds (s).

Time coverage (TimeCov) is the ratio of time frames assigned to each MS map relative to the total number of time frames from the recording. Results are Units are percentages (%) between 0 and 1.

2.5 Adjusted Mutual information score

Scikit-learn [23] implementation of the adjusted mutual information score (AMI) [24] was used to quantify the mutual information (MI) shared between different MS temporal segmentations, whilst simultaneously accounting for random overlap due to chance. This metric, bounded between 0 and 1, is used to evaluate the statistical (in)dependence of two variables. In our case, AMI is estimated between the symbolic sequences of two different microstate segmentations (e.g. ABDCADB vs ABDBDAC).

bioRxiv preprint doi: https://doi.org/10.1101/2020.10.16.342378; this version posted October 16, 2020. The copyright holder for this preprint (which was not certified by peer review) is the author/funder, who has granted bioRxiv a license to display the preprint in perpetuity. It is made available under aCC-BY 4.0 International license.

A high score (approaching 1) indicates that the two segmentations agree on the temporal order of all labels while a low score (approaching 0) indicates that the segmentations' labels are not temporally aligned. We selected the corrected version of this metric in order to control for the impact of differences in label distribution due to chance (for example differences in overall time coverage between labels).

2.6 Statistics

Statistical analyses were performed on the 4 main spatiotemporal parameters (Global explained variance, Mean spatial correlation, Mean duration, Time coverage). Tests were conducted using a two sided permutation test for equality of means on paired samples (same subject, either between condition, either between frequencies) under the H0 hypothesis that both frequency (i.e. condition) share the same mean against the alternative H1 that the distributions come from two different populations. P-values were estimated by simulated random sampling with 10000 replications. As a large number of statistical tests were carried out without specific pre-planned hypotheses [25], P values were corrected for multiple comparisons using the Bonferroni method. Corrected P-values are reported in the Results section, as well as the observed means (m) of both samples together with observed standard deviations. Effect sizes are reported as the standardised difference of means using Cohen's d (d).

bioRxiv preprint doi: https://doi.org/10.1101/2020.10.16.342378; this version posted October 16, 2020. The copyright holder for this preprint (which was not certified by peer review) is the author/funder, who has granted bioRxiv a license to display the preprint in perpetuity. It is made available under aCC-BY 4.0 International license.

3 Results

3.1 Spatial Similarity Analysis of Microstate Maps

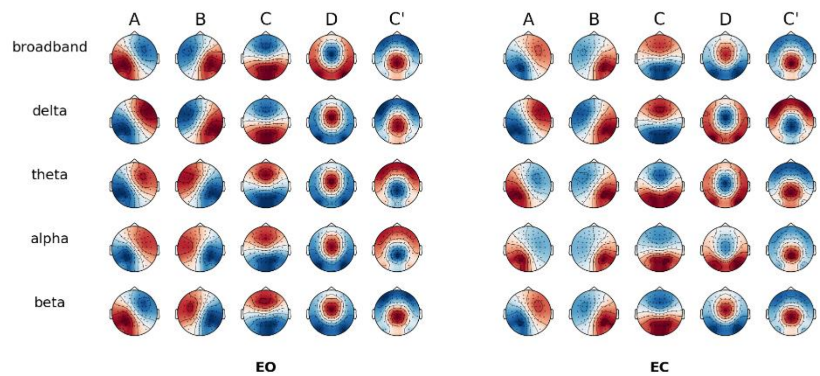

Figure 1: MS segmentation parameters of MS topographies.

Global cluster centroids of each frequency band within each condition. Note that polarity inversion is ignored in the classical analysis of spontaneous EEG.

Figure 1 illustrates the topographic results of MS segmentations in the different conditions and frequency bands. After visual inspection of optimal clusters at different cluster numbers (k), we identified that a value of k=5 revealed five MS topographies that were similar across all EEG bands and behavioural conditions, consistent with recent findings from our laboratory [21], [26], [27]. MS maps were designated in line with the canonical prototypes from the literature and their respective symbols, featuring a left-right orientation (A), a right-left orientation (B), an anterior-posterior orientation (C), fronto-central maximum (D) and occipito-central (C’)maximum.

Given the additional frequency dimension, we labelled the MS maps firstly according to the Greek letters traditionally used for narrow-band

bioRxiv preprint doi: https://doi.org/10.1101/2020.10.16.342378; this version posted October 16, 2020. The copyright holder for this preprint (which was not certified by peer review) is the author/funder, who has granted bioRxiv a license to display the preprint in perpetuity. It is made available under aCC-BY 4.0 International license.

EEG (i.e. δ, θ, α, β) and then the Latin alphabet for the canonical map symbols (i.e. A, B, C, D) . For example, αA denoted the left-right diagonal map from the alpha band (α) segmentation, and δC the anterior-posterior map from the delta band (δ) segmentation. The broadband segmentation was designated with the prefix 'bb'

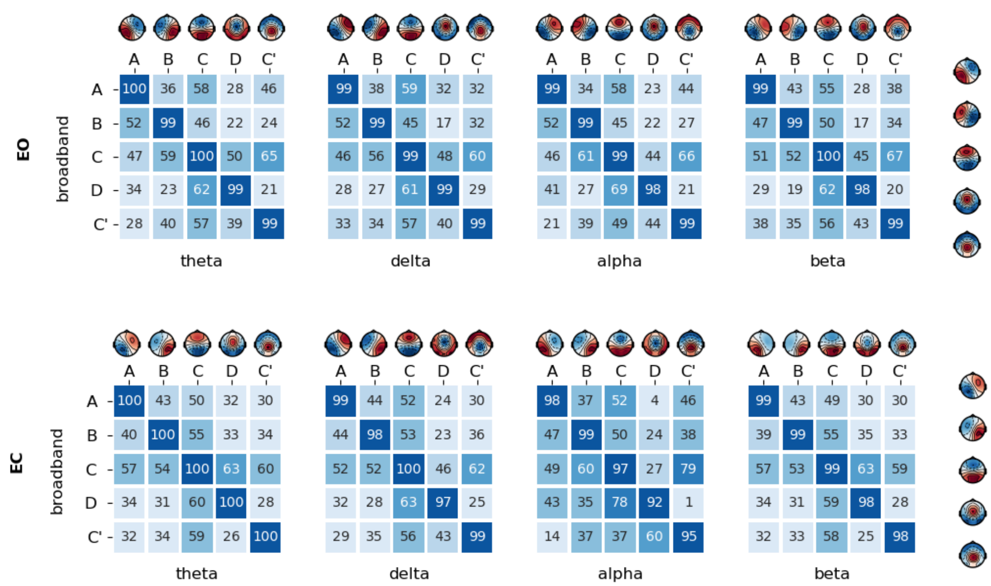

Figure 2: MS segmentation parameters of MS topographies.

Spatial correlation of cluster centers of each sub-frequency bands compared to broadband for eyes opened (EO) and eyes closed (EC) condition.

As shown in Figure 2, when comparing topographies between broadband and each narrow-band (i.e. the diagonal entries in the correlation matrix), all spatial correlations were $r > 0.98$. Consequently, we fitted the broadband maps directly to all the frequency bands in order to have a common reference.

bioRxiv preprint doi: https://doi.org/10.1101/2020.10.16.342378; this version posted October 16, 2020. The copyright holder for this preprint (which was not certified by peer review) is the author/funder, who has granted bioRxiv a license to display the preprint in perpetuity. It is made available under aCC-BY 4.0 International license.

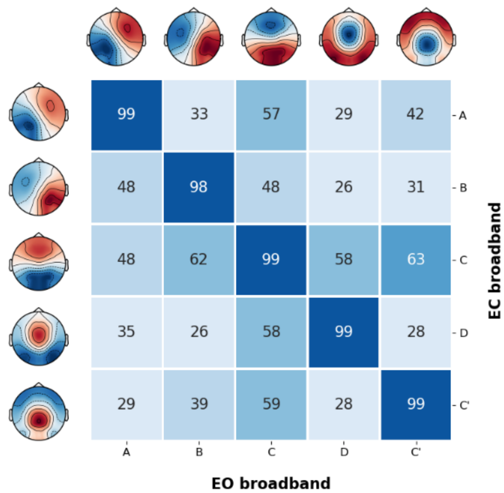

Figure 3: MS segmentation parameters of MS topographies.

Spatial correlation of broadband cluster centers between eyes opened (EO) and eyes closed (EC) condition.

We similarly observed common MS maps when comparing broadband topographies between EO and EC conditions (Figure 3), with all intraclass spatial correlations exceeding $r > 0.98$, thus providing justification for comparing microstate parameters between behavioural conditions while fitting condition specific broadband maps.

bioRxiv preprint doi: https://doi.org/10.1101/2020.10.16.342378; this version posted October 16, 2020. The copyright holder for this preprint (which was not certified by peer review) is the author/funder, who has granted bioRxiv a license to display the preprint in perpetuity. It is made available under aCC-BY 4.0 International license.

3.2 Mutual information

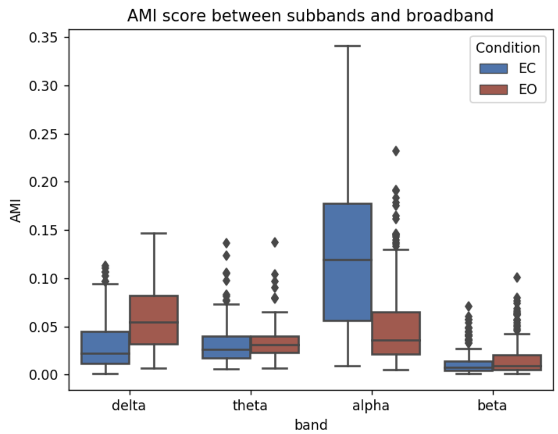

Figure 4: Adjusted mutual information between band segmentations.

Mean adjusted mutual information is depicted between broadband and narrow-band segmentations, for each behavioural condition. n = 203 subjects.

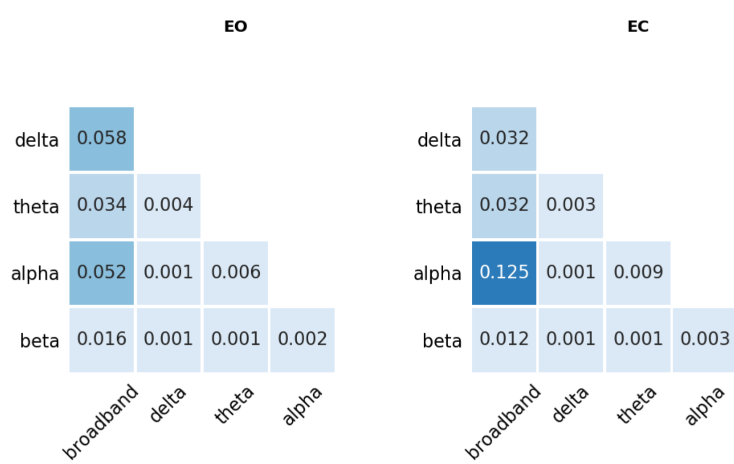

Figure 5: Mean adjusted mutual information between band segmentations.

Mean (n = 203 subjects) adjusted mutual information for all frequency pairs.

bioRxiv preprint doi: https://doi.org/10.1101/2020.10.16.342378; this version posted October 16, 2020. The copyright holder for this preprint (which was not certified by peer review) is the author/funder, who has granted bioRxiv a license to display the preprint in perpetuity. It is made available under aCC-BY 4.0 International license.

Concisely, Adjusted Mutual Information (AMI, bounded between 0 and 1) is an index of how similar two separate MS segmentations are, by estimating the degree of shared information (i.e. the number of time points assigned with the same MS) between their symbolic sequences (e.g. ABCD vs ABDA). The 'adjusted' aspect ensures the measure is unbiased for symbolic overlap(s) due to chance when cluster numbers are low (as is the case here given k=5) [24]. Higher AMI (approaching 1) indicates nearly identical MS temporal sequences, while lower AMI (approaching 0) indicates temporally independent sequences. (i.e. low overlap)

As shown in Figures 4 and 5, the AMI between broadband and narrow-band segmentations in the EO condition showed a value of s = 0.06 for delta, s = 0.03 for theta, s = 0.05 for alpha, and s = 0.01 for beta. These values are surprisingly low and we can conclude that the broadband segmentation is comparatively independent of the narrow EEG bands. A similar conclusion can be made by examining the AMI between the narrow-bands *themselves*, with a maximum AMI value between theta and alpha bands (EO: s = 0.006, EC: s = 0.009), and a minimum AMI value of s = 0.001 for non-adjacent EEG bands (delta-alpha, delta-beta, theta-beta)

As a sanity check, inspecting the EO vs EC transition, shared information with broadband decreased for the delta band (s = 0.03) but increased for the alpha band (s = 0.12). The latter is in line with predictions, as alpha oscillations are known to increase considerably during eye closure, which would amplify their contribution to the broadband signal and consequently their shared dynamics.

bioRxiv preprint doi: https://doi.org/10.1101/2020.10.16.342378; this version posted October 16, 2020. The copyright holder for this preprint (which was not certified by peer review) is the author/funder, who has granted bioRxiv a license to display the preprint in perpetuity. It is made available under aCC-BY 4.0 International license.

3.3 Across Frequency comparison

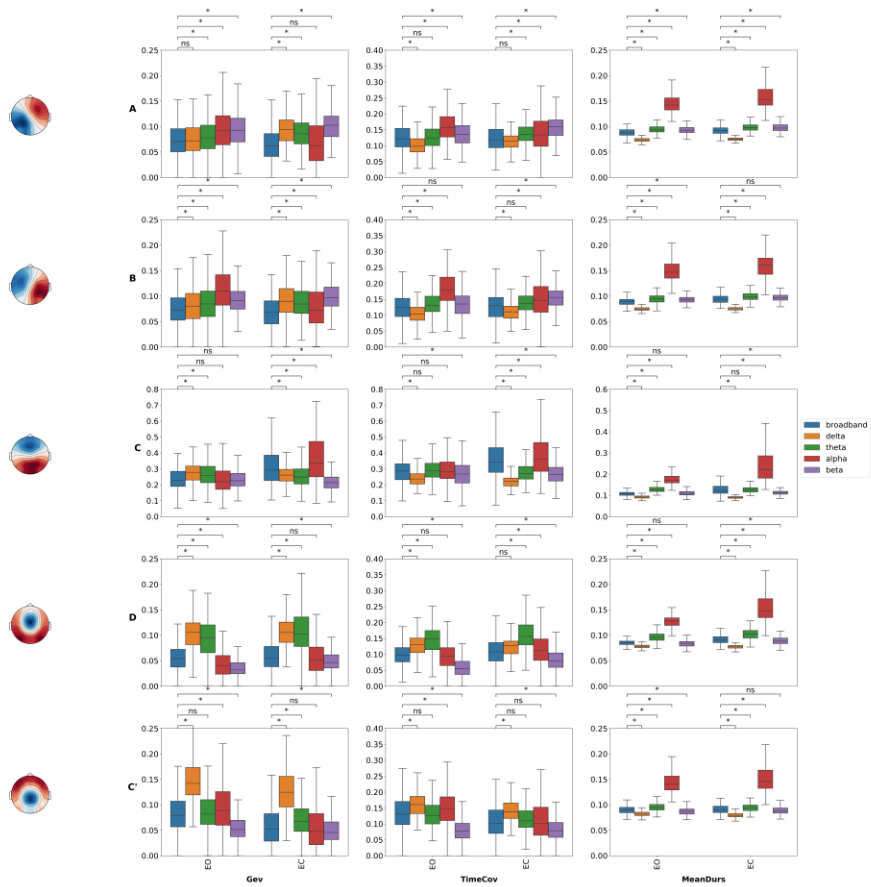

Figure 6: MS segmentation parameters of MS topographies.

Mean global explained variance (Gev), microstate time coverage (time coverage) and mean segment duration (MeanDurs, in s) within each microstate configuration (A – C') for each frequency band (broadband, delta, theta, alpha, beta) for both eyes closed condition and eyes opened condition. Significance

bioRxiv preprint doi: https://doi.org/10.1101/2020.10.16.342378; this version posted October 16, 2020. The copyright holder for this preprint (which was not certified by peer review) is the author/funder, who has granted bioRxiv a license to display the preprint in perpetuity. It is made available under aCC-BY 4.0 International license.

values are indicated from paired permutation test on mean between conditions. ns: 0.05 < p, * 0.01 < p <= 0.05.
Boxplots consist of median (Q2), first quartile (Q1), third quartile (Q3), maximum (Q3 + 1.5*(Q3 - Q1)), minimum (Q1 -1.5*((Q3 - Q1). Scales of Microstates C metrics are different from others states due to difference of order of magnitude.

All subsequent results were computed using paired permutation tests and Bonferroni correction for c = 120 comparisons. In addition to Fig 6, p-values and effect sizes are reported in Table 1 of the Supplementary Results.

In summary, only 23 of the 120 pairwise comparisons between broadband and narrow-band MS measures (Global explained variance (Gev), Mean spatial correlation, Mean duration (MeanDurs), Time coverage (TimeCov) *did not* meet the threshold for a statistical significant effect. As can be seen from Fig 6, these include Gev for δA, αC, βC, θC’, in EO and αA, αD, αC’, in EC.

TimeCov for θA, βB, θC, αC, αD, θC’, in EO and δA, θB, δD, θC’, αC’, in EC.

MeanDurs for βC, βD, in EO and βB, θC, βC’, in EC.

The majority of pairwise comparisons with broadband (97) were found to be statistically significant, some of them with large effect sizes, in particular:

In the EC condition, mean duration of map A was longer (d = 3.38, $p < 0.05$) in alpha (αA, 150 ms) compared to broadband (bbA, 90 ms). On the other hand, mean duration of map B was shorter (d = -2.08, $p < 0.05$) in delta (δB, 80 ms) compared to broadband (bbB, 90 ms), while map C duration was longer (d = 1.33, p <0 .05) in theta (θC , 130 ms) compared to

bioRxiv preprint doi: https://doi.org/10.1101/2020.10.16.342378; this version posted October 16, 2020. The copyright holder for this preprint (which was not certified by peer review) is the author/funder, who has granted bioRxiv a license to display the preprint in perpetuity. It is made available under aCC-BY 4.0 International license.

broadband (bbC, 110 ms). Relative time coverage of map D was lower (d = -1.14, $p < .05$) in beta (βD, 6 %) compared to broadband (bbD, 10%).

In the EO condition, mean duration of map B was shorter (d = -1.69, $p < 0.05$) in delta (δB, 74 ms) compared to broadband (bbB, 89 ms), but was longer (d *= 3.25,* $p < 0.05$*)* in alpha (αB, 151ms). In terms of time coverage, map D had a lower (d = -1.14, $p < 0.05$) presence in the beta band (*βD,* 5%) compared to broadband (*bbD,* 10%) while its presence was increased (d = 1.02, $p < 0.05$) in theta frequencies. *(θD 15%) Microstate C'* demonstrated more explained variance (d = -1.44, $p < 0.05$) in the delta band (*δC',* 11%) compared to broadband *(bbC', 6%)*

bioRxiv preprint doi: https://doi.org/10.1101/2020.10.16.342378; this version posted October 16, 2020. The copyright holder for this preprint (which was not certified by peer review) is the author/funder, who has granted bioRxiv a license to display the preprint in perpetuity. It is made available under aCC-BY 4.0 International license.

3.4 Within Frequency comparison

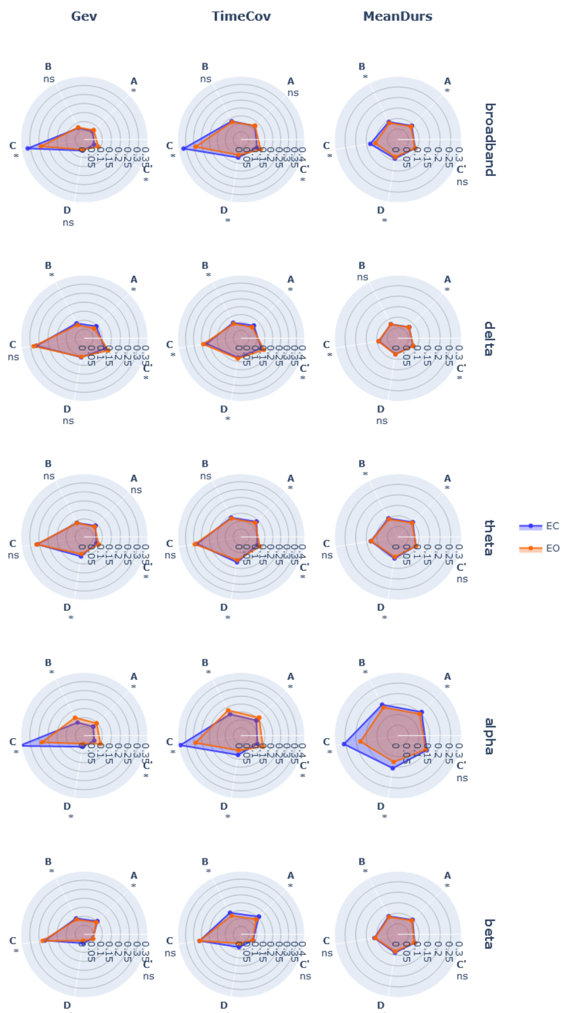

Figure 7: MS segmentation parameters of different frequency bands.

Mean global explained variance (Gev), microstate time coverage (time coverage) and mean segment duration (MeanDurs, in s) for each microstate (A – C') within each frequency band (broadband, delta, theta, alpha, beta) for both

bioRxiv preprint doi: https://doi.org/10.1101/2020.10.16.342378; this version posted October 16, 2020. The copyright holder for this preprint (which was not certified by peer review) is the author/funder, who has granted bioRxiv a license to display the preprint in perpetuity. It is made available under aCC-BY 4.0 International license.

eyes closed condition (EC, blue) and eyes opened condition (EO, red). Significance values are indicated from paired permutation test on mean between conditions.

ns : 0.05 < *p*, ∗ for 0.01 < *p* <= 0.05

In this section, we directly compared EO vs EC condition within each frequency band, and only relevant cases where narrow-band measures were distinctly different compared to the broadband analysis are reported (Figure 7). The full results are documented in Table 2 of the Supplementary Results.

For time coverage (TimeCov), map A was relatively more prevalent in EO vs EC in the alpha band (d = 0.57, $p < .05$) than for broadband (d = 0.24, $p < .05$). Conversely, map C coverage was less prevalent in alpha (sd = -1.00, $p < .05$) than broadband (d = -0.71, $p < .05$)

Some narrow-band effects were found to be opposite compared to broadband : βA TimeCov had decreased prevalence (d = -0.48, $p < .05$) in EO vs EC , while bbA TimeCov showed an increase (d = 0.24, $p < .05$). βC TimeCov had increased prevalence (d = 0.21, p <0 .05) in EO vs EC, while bbC TimeCov showed a decrease (d = -0.71, $p < .05$).

Finally significant EO vs EC effects were found in the narrow-band analyses which were not evident in the broadband case: a decrease (d = -0.31, $p < 0.05$) in Gev of map *B was observed in the beta band* while no significant effect was found for broadband. Likewise in beta, map A TimeCov was decreased (d = -0.51, p <0.05) in EO vs EC, while broadband TimeCov was non-significant (p = 1.0, n.s.).

bioRxiv preprint doi: https://doi.org/10.1101/2020.10.16.342378; this version posted October 16, 2020. The copyright holder for this preprint (which was not certified by peer review) is the author/funder, who has granted bioRxiv a license to display the preprint in perpetuity. It is made available under aCC-BY 4.0 International license.

4 Discussion

Historically, the first microstate (MS) analysis was applied by Lehmann and colleagues to narrowband (alpha) oscillations [2], yet this "frequency-specific" approach appears to have been overlooked during the last decades of MS research in favour of decomposing broadband (e.g. 2-40 Hz) EEG signals. Hence, the present study specifically explored the MS characteristics of narrow-band EEG signals, their quantitative interrelationship, and whether they provide any novel information compared to course-grained broadband dynamics. This was done by first filtering the broadband EEG signal into several narrow-band frequencies (delta, theta, alpha, and beta), with the goal of comparing MS symbolic sequences and classical measures (explained variance, mean duration, time coverage) between them, as well as across different behavioural conditions (eyes open (EO) vs eyes closed (EC)).

4.1 Topographic patterns

We first investigated whether analogous MS scalp topographies would be produced by segmenting broadband versus narrow-band EEG signals (including the alpha band [28]). Interestingly, we observed highly similar MS topographies (with minimum spatial correlations of $r > 0.98$) across all investigated broad- and narrow- band frequencies (broadband, delta to beta), as well as between EO/EC conditions. This is compatible with recent work by Brechet and colleagues [27], who observed that states of sleep and wake exhibited significantly different spectral content (e.g. delta vs beta power) but very similar MS maps. Moreover, these maps corresponded to the canonical (broadband) topographies previously described in the literature [1], [29]. It is therefore tempting to assume that

bioRxiv preprint doi: https://doi.org/10.1101/2020.10.16.342378; this version posted October 16, 2020. The copyright holder for this preprint (which was not certified by peer review) is the author/funder, who has granted bioRxiv a license to display the preprint in perpetuity. It is made available under aCC-BY 4.0 International license.

identical neuronal sources are involved in generating the same topographies across frequencies. However, although different maps imply different generators (forward problem), same topographies do not necessarily imply identical generators (inverse problem). Due to the ill-posed nature of EEG signals (constructive and destructive electromagnetic fields), similar scalp potentials can still be generated by different underlying brain mechanisms [30]. Hence, although we cannot unequivocally conclude that MS maps across the EEG spectrum are generated by the same brain sources operate, this would be the most probable and parsimonious interpretation. Moreover, we must juxtapose our findings with work from other groups [6] which applied a similar approach but didn't necessarily find the same topographies across the EEG spectrum. From a methodological point of view, it should be kept in mind that narrow-band MS analysis does not *per se* require similar topographies between frequencies. In this case, although cross frequency comparisons would not be possible due to dissimilar maps, it would remain valid to study and quantify spatiotemporal MS parameters within each frequency band separately, for example, in the service of clinical biomarker discovery [4]. Reassuringly, the MS maps of our study replicate the ones derived from independent work utilising the same EEG dataset [3], further supporting the reproducibility of MS analysis despite methodological variations between studies (e.g. absence of resampling).

4.2 Mutual information

Milz and colleagues [28] recently proposed that alpha oscillations were the major component driving microstate dynamics. In general, adjusted mutual information (AMI) analyses reported in our work reveal low values (near or below 0.1) of information shared between the narrow-band segmentations, including alpha, and that of the broadband

bioRxiv preprint doi: https://doi.org/10.1101/2020.10.16.342378; this version posted October 16, 2020. The copyright holder for this preprint (which was not certified by peer review) is the author/funder, who has granted bioRxiv a license to display the preprint in perpetuity. It is made available under aCC-BY 4.0 International license.

decomposition. However, consistent with the work of Milz and colleagues [28], the alpha-band during eyes-closed (EC) did indeed have the highest shared information with broadband (around 0.125). Importantly however, this relationship did not necessarily hold during eyes-open (delta being highest). This indicates specific narrow-band contribution(s) to broadband dynamics heavily depend on behavioural state. Moreover, if narrow-band(s) topographies were directly responsible for the origin of the spatial distribution of the broadband signal, one would expect much higher AMI values (at least 0.5) than those, we observed. In view of the results presented, it would be inaccurate to claim that alpha band, or any other narrow-band as the dominant source of broadband topographies.

In contrast, our results appear to support the ideas of Croce and colleagues [31], who suggested that broadband MS dynamics could not be extrapolated from one or a subset of EEG frequency bands. It remains unclear how the interaction of several narrow-band-components leads to a substantially different broadband MS decomposition. We speculate that this might stem from the fact that i) different narrow band signals could cancel each other at specific time points and ii) microstate assignment is non-linear given the winner-takes all approach.

Lastly and most intriguingly, no significant informational interrelations were found between the narrow-band topographical dynamics themselves (e.g. delta vs beta, theta vs alpha), indicating that each EEG band appears to have has its own independent dynamics. This may not be surprising, considering that spontaneous EEG oscillations have been reported to dynamically switch from a resting signatures (e.g. alpha) to task-specific active mode(s) dominated by theta [11], beta [32] or gamma activities [12]). In this context, our observations of spatiotemporal independence between narrow-band EEG components support the operation of “oscillatory multiplexing” [13] mechanisms in the cortex,

bioRxiv preprint doi: https://doi.org/10.1101/2020.10.16.342378; this version posted October 16, 2020. The copyright holder for this preprint (which was not certified by peer review) is the author/funder, who has granted bioRxiv a license to display the preprint in perpetuity. It is made available under aCC-BY 4.0 International license.

whereby brain regions could combine different frequencies for integrating/segregating information across large-scale networks [33]

4.3 Classical microstate parameters

Microstates are defined as short periods of time during which the scalp electric field remains quasi-stable. Traditional microstate analysis does not suggest specific frequency filtering, thus resulting in various filters settings across studies [1]. Our findings show that quasi stable structures (around 80ms or longer) are present in all studied bands. It is established that such spatiotemporal structures do not appear for randomly shuffled EEG [34]. For most EEG narrow-bands, mean MS durations were usually in the same range as the typically reported 70–120 ms, but often longer (for example, alpha in EC was about 150 ms). It is therefore interesting to consider the mechanistic links between the course-grained broadband dynamics of the brain's microstates and the dynamics of different frequency-specific modes.

4.4 Between condition comparison: toward a systematic frequency decomposition of microstate dynamics?

A total of about one third (22 of 75) of pairwise comparisons between eyes open and eyes closed conditions revealed significant effects. Within each frequency, between 14 (for alpha) and 8 (for theta) of the studied parameters were found significant. Compared to the narrow-band results, the classical broadband MS parameters had a higher effect size for only one parameter (broadband microstate B mean duration). For all other 14

bioRxiv preprint doi: https://doi.org/10.1101/2020.10.16.342378; this version posted October 16, 2020. The copyright holder for this preprint (which was not certified by peer review) is the author/funder, who has granted bioRxiv a license to display the preprint in perpetuity. It is made available under aCC-BY 4.0 International license.

parameters, at least one narrow-band component showed a relatively stronger effect size.

The addition of the frequency dimension therefore has the primary benefit of increasing the number of potential markers that could aid clinical prognosis or for the understanding of brain mechanisms. Hence, the extra frequency dimension could in itself lead to more fine-grained explorations of the multiplex EEG signal than the more general broadband analysis. It remains for future work to investigate the statistical power and effect sizes of these markers compared to those studied traditionally.

Moreover, narrow-band effects were sometimes found to be opposite to the broadband analysis, hence limiting the analysis to the latter could lead to incorrect or incomplete interpretations of underlying brain dynamics. We expect that future studies will explore the neurophysiological significance of narrowband MS analysis more deeply.

4.5 Potential Limitations and Future Work

We consider to current findings exploratory, considering the large number of tests that were carried out and in the absence of well-defined hypotheses. Nevertheless, we carried out Bonferroni correction, which may be considered the most conservative method for controlling multiple comparisons. Several studies have thus far proposed explanations for the origins of broadband MS topographies [7]. We feel it is still too early to make analogies or speculations between these results and those of the narrow-band dynamics. However, we believe that the application of the methodology proposed here may lead to valuable insights in order to more fully understand the underlying spectral tapestry of EEG microstates.

bioRxiv preprint doi: https://doi.org/10.1101/2020.10.16.342378; this version posted October 16, 2020. The copyright holder for this preprint (which was not certified by peer review) is the author/funder, who has granted bioRxiv a license to display the preprint in perpetuity. It is made available under aCC-BY 4.0 International license.

5 Conclusion

Ultimately, we report a number of important new findings between the classical broadband MS analysis, usually performed in the EEG field, and its application to more narrow frequency bands relevant to cortical oscillatory activities. In a nutshell, it appears that each canonical EEG frequency band possesses its own spatiotemporal dynamics, and that broadband dynamics cannot be appropriately explained by individual narrow-band frequency components.

Analysis of narrow-band MS parameters revealed spatial and temporal characteristics that both converged and diverged from broadband MS findings. At the very least, our results indicate that narrow-band analysis is justified as complementary to the usual broadband MS analysis. A narrow-band decomposition into frequencies more specific for cortical oscillatory activity could not only advance and/or consolidate findings in clinical disorders e.g. [4] [6], but also enable a better understanding of the organization and functioning of large-scale brain dynamics.

Credit authorship contribution statement

Victor Férat: Conceptualization, Formal analysis, Methodology, Visualization, Writing - original draft, Writing - review & editing.
Martin Seeber: Writing - review & editing
Christoph Michel: Writing - review & editing
Tomas Ros: Writing **-** Conceptualization, Formal analysis, Methodology review & editing**.**

Acknowledgments

bioRxiv preprint doi: https://doi.org/10.1101/2020.10.16.342378; this version posted October 16, 2020. The copyright holder for this preprint (which was not certified by peer review) is the author/funder, who has granted bioRxiv a license to display the preprint in perpetuity. It is made available under aCC-BY 4.0 International license.

We would like to thank the Mind-Body-Emotion group at the Max Planck Institute for Human Cognitive and Brain Sciences for all the work they have done to make their dataset public.

The study was supported by the Swiss National Science Foundation (NCCR Synapsy grant No. 51NF40 – 185897 and grant No. 320030_184677) to CMM.

Conflict of Interest Statement

The authors declare that the research was conducted in the absence of any commercial or financial relationships that could be construed as a potential conflict of interest.

References

[1] C. M. Michel and T. Koenig, 'EEG microstates as a tool for studying the temporal dynamics of whole-brain neuronal networks: A review', *NeuroImage*, vol. 180, pp. 577–593, Oct. 2018, doi: 10.1016/j.neuroimage.2017.11.062.

[2] D. Lehmann, 'Multichannel topography of human alpha EEG fields', *Electroencephalogr. Clin. Neurophysiol.*, vol. 31, no. 5, pp. 439–449, 1971.

[3] A. P. Zanesco, B. G. King, A. C. Skwara, and C. D. Saron, 'Within and between-person correlates of the temporal dynamics of resting EEG microstates', *NeuroImage*, vol. 211, p. 116631, May 2020, doi: 10.1016/j.neuroimage.2020.116631.

[4] E. L. Merrin, P. Meek, T. C. Floyd, and E. Callaway III, 'Topographic segmentation of waking EEG in medication-free schizophrenic patients', *Int. J. Psychophysiol.*, vol. 9, no. 3, pp. 231–236, 1990.

[5] E. Javed, P. Croce, F. Zappasodi, and C. Del Gratta, 'Hilbert spectral analysis of EEG data reveals spectral dynamics associated with microstates', *J. Neurosci. Methods*, vol. 325, p. 108317, 2019.

[6] C. S. Musaeus *et al.*, 'Changes in the left temporal microstate are a sign of cognitive decline in patients with Alzheimer's disease', *Brain Behav.*, p. e01630, 2020.

[7] J. Britz, D. Van De Ville, and C. M. Michel, 'BOLD correlates of EEG topography reveal rapid resting-state network dynamics',

bioRxiv preprint doi: https://doi.org/10.1101/2020.10.16.342378; this version posted October 16, 2020. The copyright holder for this preprint (which was not certified by peer review) is the author/funder, who has granted bioRxiv a license to display the preprint in perpetuity. It is made available under aCC-BY 4.0 International license.

NeuroImage, vol. 52, no. 4, pp. 1162–1170, Oct. 2010, doi: 10.1016/j.neuroimage.2010.02.052.

[8] D. M. Groppe *et al.*, 'Dominant frequencies of resting human brain activity as measured by the electrocorticogram', *NeuroImage*, vol. 79, pp. 223–233, Oct. 2013, doi: 10.1016/j.neuroimage.2013.04.044.

[9] M. S. Mellem, S. Wohltjen, S. J. Gotts, A. S. Ghuman, and A. Martin, 'Intrinsic frequency biases and profiles across human cortex', *J. Neurophysiol.*, vol. 118, no. 5, pp. 2853–2864, 2017.

[10] A. Keitel and J. Gross, 'Individual human brain areas can be identified from their characteristic spectral activation fingerprints', *PLoS Biol.*, vol. 14, no. 6, p. e1002498, 2016.

[11] U. Ribary, S. M. Doesburg, and L. M. Ward, 'Unified principles of thalamo-cortical processing: the neural switch', *Biomed. Eng. Lett.*, vol. 7, no. 3, pp. 229–235, Aug. 2017, doi: 10.1007/s13534-017-0033-4.

[12] J. F. Hipp, A. K. Engel, and M. Siegel, 'Oscillatory Synchronization in Large-Scale Cortical Networks Predicts Perception', *Neuron*, vol. 69, no. 2, pp. 387–396, Jan. 2011, doi: 10.1016/j.neuron.2010.12.027.

[13] T. Akam and D. M. Kullmann, 'Oscillatory multiplexing of population codes for selective communication in the mammalian brain', *Nat. Rev. Neurosci.*, vol. 15, no. 2, pp. 111–122, Feb. 2014, doi: 10.1038/nrn3668.

[14] J. J. Schulman, R. Cancro, S. Lowe, F. Lu, K. D. Walton, and R. R. Llinás, 'Imaging of Thalamocortical Dysrhythmia in Neuropsychiatry', *Front. Hum. Neurosci.*, vol. 5, 2011, doi: 10.3389/fnhum.2011.00069.

[15] T. Ros *et al.*, 'Neurofeedback Tunes Scale-Free Dynamics in Spontaneous Brain Activity', *Cereb. Cortex*, p. cercor;bhw285v1, Sep. 2016, doi: 10.1093/cercor/bhw285.

[16] A. Babayan *et al.*, 'A mind-brain-body dataset of MRI, EEG, cognition, emotion, and peripheral physiology in young and old adults', *Sci. Data*, vol. 6, p. 180308, 2019.

[17] R. D. Pascual-Marqui, C. M. Michel, and D. Lehmann, 'Segmentation of brain electrical activity into microstates: model estimation and validation', *IEEE Trans. Biomed. Eng.*, vol. 42, no. 7, pp. 658–665, 1995.

[18] A. Gramfort *et al.*, 'MEG and EEG data analysis with MNE-Python', *Front. Neurosci.*, vol. 7, p. 267, 2013.

[19] T. Koenig and D. Brandeis, 'Inappropriate assumptions about EEG state changes and their impact on the quantification of EEG state dynamics', *Neuroimage*, vol. 125, pp. 1104–1106, 2016.

[20] D. Brunet, M. M. Murray, and C. M. Michel, 'Spatiotemporal analysis of multichannel EEG: CARTOOL', *Comput. Intell. Neurosci.*, vol. 2011, 2011.

bioRxiv preprint doi: https://doi.org/10.1101/2020.10.16.342378; this version posted October 16, 2020. The copyright holder for this preprint (which was not certified by peer review) is the author/funder, who has granted bioRxiv a license to display the preprint in perpetuity. It is made available under aCC-BY 4.0 International license.

[21] L. Bréchet, D. Brunet, G. Birot, R. Gruetter, C. M. Michel, and J. Jorge, 'Capturing the spatiotemporal dynamics of self-generated, task-initiated thoughts with EEG and fMRI', *Neuroimage*, vol. 194, pp. 82–92, 2019.

[22] D. Van De Ville, J. Britz, and C. M. Michel, 'EEG microstate sequences in healthy humans at rest reveal scale-free dynamics', *Proc. Natl. Acad. Sci.*, vol. 107, no. 42, pp. 18179–18184, Oct. 2010, doi: 10.1073/pnas.1007841107.

[23] F. Pedregosa *et al.*, 'Scikit-learn: Machine Learning in Python', *J. Mach. Learn. Res.*, vol. 12, pp. 2825–2830, 2011.

[24] N. X. Vinh, J. Epps, and J. Bailey, 'Information theoretic measures for clusterings comparison: Variants, properties, normalization and correction for chance', *J. Mach. Learn. Res.*, vol. 11, pp. 2837–2854, 2010.

[25] R. A. Armstrong, 'When to use the B onferroni correction', *Ophthalmic Physiol. Opt.*, vol. 34, no. 5, pp. 502–508, 2014.

[26] D. F. D'Croz-Baron, M. Baker, C. M. Michel, and T. Karp, 'EEG Microstates Analysis in Young Adults With Autism Spectrum Disorder During Resting-State', *Front. Hum. Neurosci.*, vol. 13, p. 173, Jun. 2019, doi: 10.3389/fnhum.2019.00173.

[27] L. Bréchet, D. Brunet, L. Perogamvros, G. Tononi, and C. M. Michel, 'EEG microstates of dreams', *Sci. Rep.*, vol. 10, no. 1, p. 17069, Dec. 2020, doi: 10.1038/s41598-020-74075-z.

[28] P. Milz, R. D. Pascual-Marqui, P. Achermann, K. Kochi, and P. L. Faber, 'The EEG microstate topography is predominantly determined by intracortical sources in the alpha band', *Neuroimage*, vol. 162, pp. 353–361, 2017.

[29] A. Custo, D. Van De Ville, W. M. Wells, M. I. Tomescu, D. Brunet, and C. M. Michel, 'Electroencephalographic resting-state networks: source localization of microstates', *Brain Connect.*, vol. 7, no. 10, pp. 671–682, 2017.

[30] H. von Helmholtz, 'Ueber einige Gesetze der Vertheilung elektrischer Strome in korperlichen Leitern, mit Anwendung auf die thierisch-elektrischen Versuche (Schluss.)', *Ann. Phys.*, vol. 165, no. 7, pp. 353–377, 1853.

[31] P. Croce, A. Quercia, S. Costa, and F. Zappasodi, 'EEG microstates associated with intra-and inter-subject alpha variability', *Sci. Rep.*, vol. 10, no. 1, pp. 1–11, 2020.

[32] T. Fernández *et al.*, 'EEG activation patterns during the performance of tasks involving different components of mental calculation', *Electroencephalogr. Clin. Neurophysiol.*, vol. 94, no. 3, pp. 175–182, Mar. 1995, doi: 10.1016/0013-4694(94)00262-J.

bioRxiv preprint doi: https://doi.org/10.1101/2020.10.16.342378; this version posted October 16, 2020. The copyright holder for this preprint (which was not certified by peer review) is the author/funder, who has granted bioRxiv a license to display the preprint in perpetuity. It is made available under aCC-BY 4.0 International license.

[33] M. Le Van Quyen, 'The brainweb of cross-scale interactions', *New Ideas Psychol.*, vol. 29, no. 2, pp. 57–63, Aug. 2011, doi: 10.1016/j.newideapsych.2010.11.001.
[34] J. Wackermann, D. Lehmann, C. Michel, and W. Strik, 'Adaptive segmentation of spontaneous EEG map series into spatially defined microstates', *Int. J. Psychophysiol.*, vol. 14, no. 3, pp. 269–283, 1993.

bioRxiv preprint doi: https://doi.org/10.1101/2020.10.16.342378; this version posted October 16, 2020. The copyright holder for this preprint (which was not certified by peer review) is the author/funder, who has granted bioRxiv a license to display the preprint in perpetuity. It is made available under aCC-BY 4.0 International license.

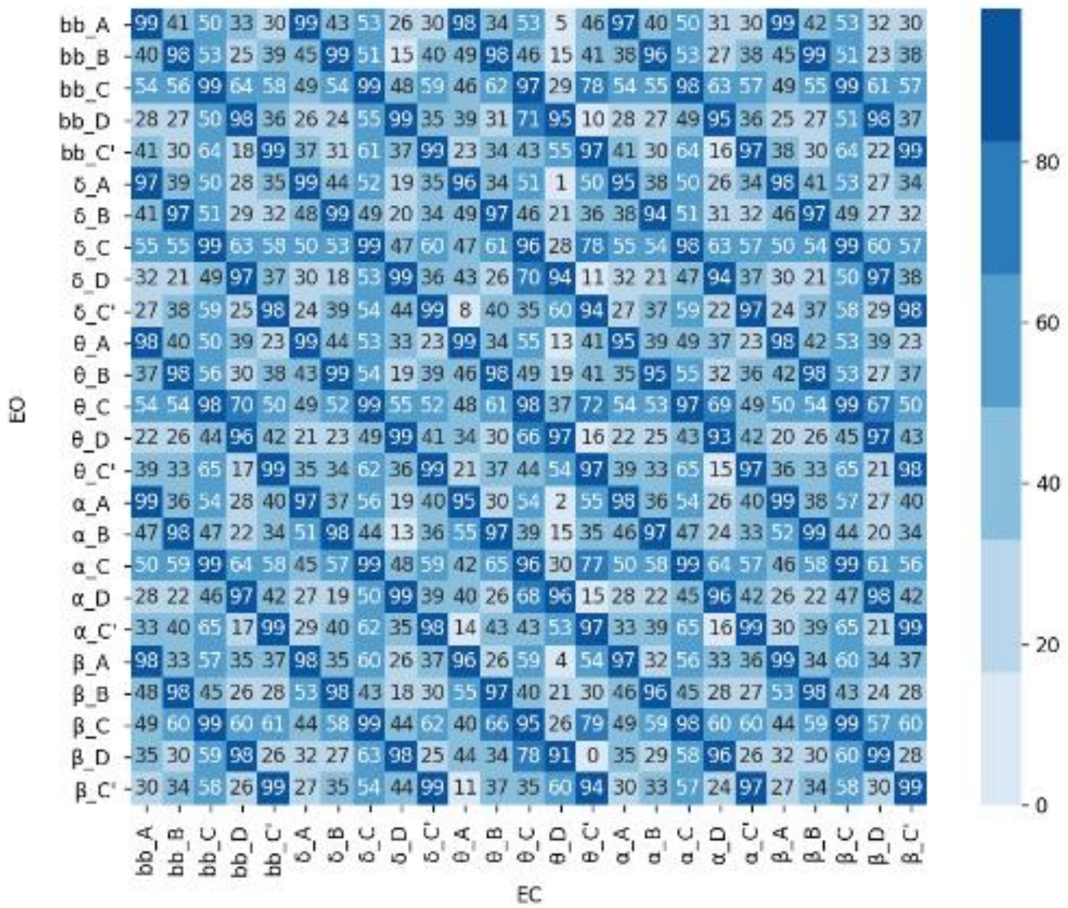

Figure : MS segmentation parameters of MS topographies.

Spatial correlation of cluster centers between eyes opened (EO) and eyes closed (EC) condition across all frequency bands.

bioRxiv preprint doi: https://doi.org/10.1101/2020.10.16.342378; this version posted October 16, 2020. The copyright holder for this preprint (which was not certified by peer review) is the author/funder, who has granted bioRxiv a license to display the preprint in perpetuity. It is made available under aCC-BY 4.0 International license.

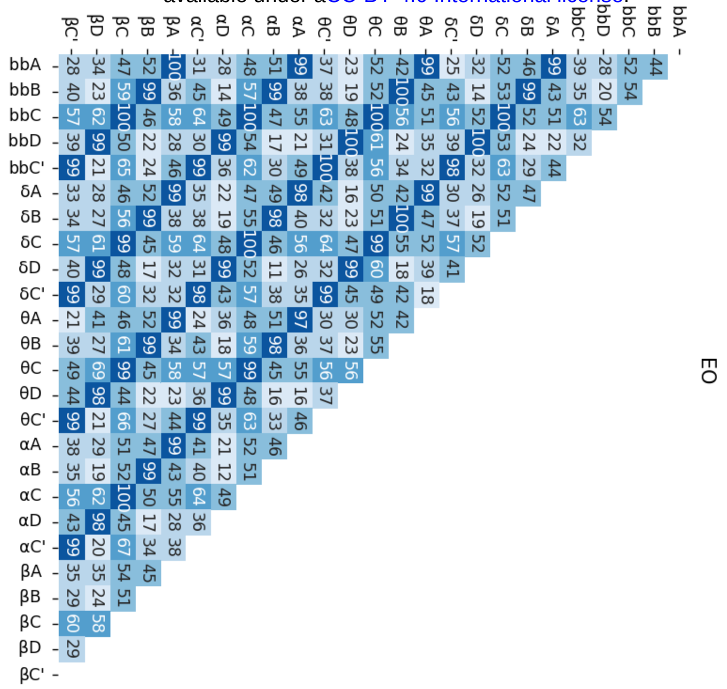

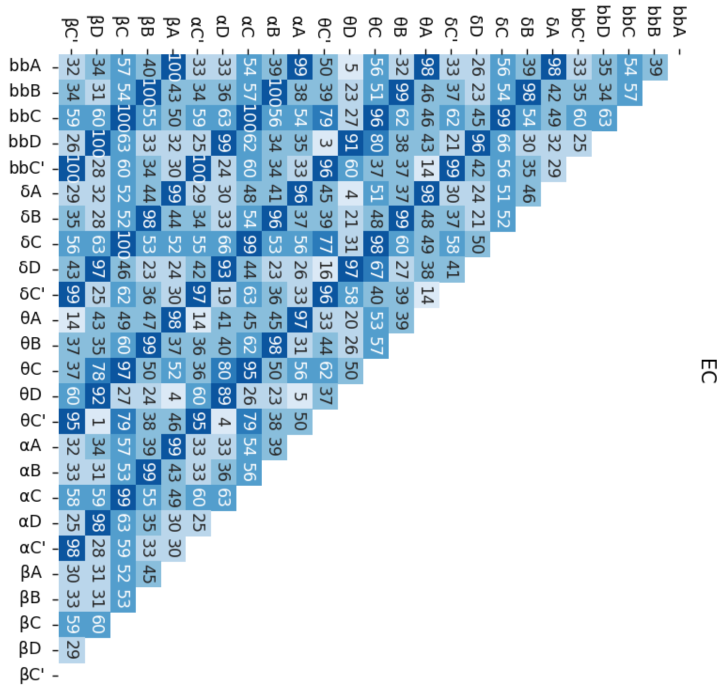

Figure: MS segmentation parameters of MS topographies.
Spatial correlation of cluster centers between all frequency bands in both EO and EC conditions.

bioRxiv preprint doi: https://doi.org/10.1101/2020.10.16.342378; this version posted October 16, 2020. The copyright holder for this preprint (which was not certified by peer review) is the author/funder, who has granted bioRxiv a license to display the preprint in perpetuity. It is made available under aCC-BY 4.0 International license.

EO

map	band1	metric	d	p
A	alpha	Gev	0.57	0.02
		MeanDurs	3.38	0.02
		TimeCov	0.76	0.02
	beta	Gev	0.61	0.02
		MeanDurs	0.47	0.02
		TimeCov	0.23	0.02
	delta	Gev	0.11	1.00
		MeanDurs	-1.80	0.02
		TimeCov	-0.66	0.02
	theta	Gev	0.22	0.02
		MeanDurs	0.62	0.02
		TimeCov	0.05	1.00
B	alpha	Gev	0.94	0.02
		MeanDurs	3.25	0.02
		TimeCov	1.13	0.02
	beta	Gev	0.56	0.02
		MeanDurs	0.37	0.02
		TimeCov	0.18	0.17
	delta	Gev	0.20	0.05
		MeanDurs	-1.69	0.02
		TimeCov	-0.56	0.02
	theta	Gev	0.32	0.02
		MeanDurs	0.58	0.02
		TimeCov	0.17	0.05
C	alpha	Gev	-0.06	1.00
		MeanDurs	2.31	0.02
		TimeCov	0.00	1.00
	beta	Gev	-0.13	1.00
		MeanDurs	0.10	1.00
		TimeCov	-0.30	0.02
	delta	Gev	0.50	0.02
		MeanDurs	-1.28	0.02
		TimeCov	-0.71	0.02
	theta	Gev	0.31	0.02
		MeanDurs	1.33	0.02
		TimeCov	0.06	1.00
C'	alpha	Gev	0.25	0.02
		MeanDurs	2.41	0.02
		TimeCov	0.25	0.02
	beta	Gev	-0.87	0.02
		MeanDurs	-0.30	0.02
		TimeCov	-1.10	0.02
	delta	Gev	1.32	0.02
		MeanDurs	-0.91	0.02
		TimeCov	0.45	0.02
	theta	Gev	0.06	1.00
		MeanDurs	0.52	0.02
		TimeCov	-0.12	1.00
D	alpha	Gev	-0.40	0.02
		MeanDurs	3.23	0.02
		TimeCov	-0.11	1.00
	beta	Gev	-0.91	0.02
		MeanDurs	-0.17	0.60
		TimeCov	-1.14	0.02
	delta	Gev	1.44	0.02
		MeanDurs	-0.91	0.02
		TimeCov	0.81	0.02
	theta	Gev	1.06	0.02
		MeanDurs	1.06	0.02
		TimeCov	1.02	0.02

EC

map	band1	metric	d	p
A	alpha	Gev	0.12	0.10
		MeanDurs	3.25	0.02
		TimeCov	0.28	0.02
	beta	Gev	1.12	0.02
		MeanDurs	0.44	0.02
		TimeCov	0.83	0.02
	delta	Gev	0.88	0.02
		MeanDurs	-2.00	0.02
		TimeCov	-0.24	0.14
	theta	Gev	0.66	0.02
		MeanDurs	0.55	0.02
		TimeCov	0.38	0.02
B	alpha	Gev	0.22	0.02
		MeanDurs	2.91	0.02
		TimeCov	0.38	0.02
	beta	Gev	0.82	0.02
		MeanDurs	0.19	0.14
		TimeCov	0.48	0.02
	delta	Gev	0.60	0.02
		MeanDurs	-2.08	0.02
		TimeCov	-0.49	0.02
	theta	Gev	0.46	0.02
		MeanDurs	0.43	0.02
		TimeCov	0.16	0.48
C	alpha	Gev	0.34	0.02
		MeanDurs	1.50	0.02
		TimeCov	0.16	0.02
	beta	Gev	-1.00	0.02
		MeanDurs	-0.76	0.02
		TimeCov	-1.00	0.02
	delta	Gev	-0.48	0.02
		MeanDurs	-1.64	0.02
		TimeCov	-1.53	0.02
	theta	Gev	-0.50	0.02
		MeanDurs	-0.08	1.00
		TimeCov	-0.83	0.02
C'	alpha	Gev	0.00	1.00
		MeanDurs	2.50	0.02
		TimeCov	0.05	1.00
	beta	Gev	-0.24	0.02
		MeanDurs	-0.20	0.24
		TimeCov	-0.54	0.02
	delta	Gev	1.52	0.02
		MeanDurs	-1.17	0.02
		TimeCov	0.63	0.02
	theta	Gev	0.31	0.02
		MeanDurs	0.31	0.02
		TimeCov	0.07	1.00
D	alpha	Gev	0.02	1.00
		MeanDurs	2.44	0.02
		TimeCov	0.14	0.02
	beta	Gev	-0.40	0.02
		MeanDurs	-0.30	0.02
		TimeCov	-0.73	0.02
	delta	Gev	1.26	0.02
		MeanDurs	-1.47	0.02
		TimeCov	0.17	1.00
	theta	Gev	1.15	0.02
		MeanDurs	0.81	0.02
		TimeCov	0.87	0.02

Table 1: For both EO and EC condition, P values (p) and cohen's d (d) are reported for each test between broadband and band segmentation on each studied metric (Global explained variance, Mean duration, time coverage).

bioRxiv preprint doi: https://doi.org/10.1101/2020.10.16.342378; this version posted October 16, 2020. The copyright holder for this preprint (which was not certified by peer review) is the author/funder, who has granted bioRxiv a license to display the preprint in perpetuity. It is made available under aCC-BY 4.0 International license.

map	band	metric	d	p
A	alpha	Gev	0.12	0.10
		MeanDurs	3.25	0.02
		TimeCov	0.28	0.02
	beta	Gev	1.12	0.02
		MeanDurs	0.44	0.02
		TimeCov	0.83	0.02
	delta	Gev	0.88	0.02
		MeanDurs	-2.00	0.02
		TimeCov	-0.24	0.14
	theta	Gev	0.66	0.02
		MeanDurs	0.55	0.02
		TimeCov	0.38	0.02
B	alpha	Gev	0.22	0.02
		MeanDurs	2.91	0.02
		TimeCov	0.38	0.02
	beta	Gev	0.82	0.02
		MeanDurs	0.19	0.14
		TimeCov	0.48	0.02
	delta	Gev	0.60	0.02
		MeanDurs	-2.08	0.02
		TimeCov	-0.49	0.02
	theta	Gev	0.46	0.02
		MeanDurs	0.43	0.02
		TimeCov	0.16	0.48
C	alpha	Gev	0.34	0.02
		MeanDurs	1.50	0.02
		TimeCov	0.16	0.02
	beta	Gev	-1.00	0.02
		MeanDurs	-0.76	0.02
		TimeCov	-1.00	0.02
	delta	Gev	-0.48	0.02
		MeanDurs	-1.64	0.02
		TimeCov	-1.53	0.02
	theta	Gev	-0.50	0.02
		MeanDurs	-0.08	1.00
		TimeCov	-0.83	0.02
C'	alpha	Gev	0.00	1.00
		MeanDurs	2.50	0.02
		TimeCov	0.05	1.00
	beta	Gev	-0.24	0.02
		MeanDurs	-0.20	0.24
		TimeCov	-0.54	0.02
	delta	Gev	1.52	0.02
		MeanDurs	-1.17	0.02
		TimeCov	0.63	0.02
	theta	Gev	0.31	0.02
		MeanDurs	0.31	0.02
		TimeCov	0.07	1.00
D	alpha	Gev	0.02	1.00
		MeanDurs	2.44	0.02
		TimeCov	0.14	0.02
	beta	Gev	-0.40	0.02
		MeanDurs	-0.30	0.02
		TimeCov	-0.73	0.02
	delta	Gev	1.26	0.02
		MeanDurs	-1.47	0.02
		TimeCov	0.17	1.00
	theta	Gev	1.15	0.02
		MeanDurs	0.81	0.02
		TimeCov	0.87	0.02

Table 2: For each between conditions (EO/EC) test P values (p) and cohen's d (d) are reported for all combinations of band, map and metric.